

Observation of Stepwise Ultrafast Crystallization Kinetics of Donor–Acceptor Conjugated Polymers and Correlation with Field Effect Mobility

Shaochuan Luo, Nan Li, Song Zhang, Chen Zhang, Tengfei Qu, Michael U. Ocheje, Gi Xue, Xiaodan Gu, Simon Rondeau-Gagné, Wenbing Hu, Sihong Wang, Chao Teng,* Dongshan Zhou,* and Jie Xu*



Cite This: <https://dx.doi.org/10.1021/acs.chemmater.0c03854>



Read Online

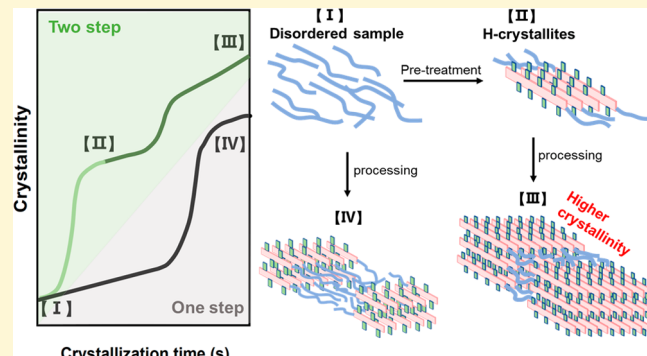
ACCESS |

Metrics & More

Article Recommendations

Supporting Information

ABSTRACT: The semicrystalline microstructures of donor–acceptor conjugated polymers strongly impact their optoelectronic properties. The control of the microstructure relies on the understandings of the crystallization processes in these polymers, from packing structures to crystallization kinetics. How fast these conjugated polymer chains crystallize and how their chemical structures and pre-existing microstructure history influence their crystallization have so far remained unclear, due to the fast crystallization rate caused by chain rigid structures and strong interactions. Here, ultrafast scanning calorimetry (FSC) is employed to reveal the crystallization behaviors of high performance diketopyrrolopyrrole (DPP)-based conjugated polymers with scanning rates up to 500 000 K/s. Through elaborately designed nonisothermal and isothermal crystallization studies, we probed the fast crystallization kinetics and extracted the two-step crystallization process of these polymers quantitatively. We found that both the rigidity of the chain backbones and the preinduced crystalline microstructures can influence the crystallization rate over an order of magnitude at the same degree of undercooling. We further demonstrated the manipulated crystallization kinetics in the DPP-based polymer films with different amounts of preinduced crystallites and correlate it to the polymers’ charge transport mobility.



INTRODUCTION

Conjugated polymers with interesting optical, electrical, and mechanical properties are strongly desired for a vast range of applications including flexible light-emitting diodes, printable photovoltaics, wearable electronics, and sensory technologies.^{1–4} These polymers have chemical structures endowed with a π -electron conjugation along the polymer backbone and usually form into semicrystalline microstructures. Their chemical structures primarily dictate their solid-state properties,^{5–8} while the physical packing structures of polymer chains also play a critical role.^{9–14} For example, improved crystallinity in conjugated polymer films through annealing can lead to more than 1 order of magnitude improvement in charge-transport mobility,^{15–17} while the suppressed growth of large crystallites in conjugated polymers results in significant improvement in mechanical stretchability.^{1,18} However, the crystallization behaviors (e.g., the crystallization kinetics and the crystal growth) of conjugated polymers and their correlations with the chemical and morphological structures are still awaiting further understanding.^{19–22}

The evolution of conjugated polymer crystallization typically consists of two processes: (1) the formation of primary nuclei or aggregates and (2) the crystal growth. There have been many processing methods developed to modulate the crystallization of conjugated polymers, such as thermal annealing,^{23,24} pretreatments of polymer solutions,^{21,25} and advanced deposition methods (e.g., shear coating,^{26,27} template modification,²⁸ and slow solvent evaporation²⁹). During these crystallization processes, the complex intra/intermolecular forces (e.g., intrachain flexibility constraints and interchain π – π interactions) and pre-existing structure history (e.g., local aggregation and anisotropic crystallites) will both impact the evolution of the crystal structures and, thus, influence the solid-state properties (e.g., electrical, mechanical). To understand

Received: September 29, 2020

Revised: February 2, 2021

the crystallization mechanism of conjugated polymers, many efforts have been made through morphological characterizations (e.g., X-ray based scattering and atomic force microscope (AFM))^{15,17,30,31} and thermal analysis (e.g., differential scanning calorimetry (DSC)).^{32–34} For instance, Segalman et al.¹⁵ employed the grazing-incidence X-ray diffraction and ultraviolet-visible (UV-vis) spectroscopy to study the time-resolved crystallization in poly(3-alkylthiophene). Muller et al.³³ explored the nucleation and crystal growth of P3EHT through Avrami analysis by DSC isothermal study. As the characterizations performed in these studies are in the time scale of minutes to hours and generally provided the averaged information on all the crystalline regions, the formation of primary nanocrystalline/nuclei³⁵ in the time scale of milliseconds or less and the detailed fingerprint of individual lamellar stacks remain unexplored but are essential for understanding the resulted microstructures. In addition, the time-resolved probing of the crystallization kinetics could provide the time scales of polymer chain rearrangements under selected conditions and, thus, lead to temporal design rules for the processing of semiconducting polymer thin films.

It has been challenging to probe the crystallization kinetics in conjugated polymers, because their strong intermolecular forces and stiff chain backbones generate a strong tendency for them to aggregate, thereby leading to an ultrafast crystallization rate. DSC is the most common characterization method for the studies of crystallization behaviors. The crystallinity and the crystal size can be investigated by analyzing the melting peak from the scanning curves, while the crystallization kinetics can be probed by studying the endothermic and exothermic peaks through the nonisothermal crystallization study and analyzing the crystallization half time and Avrami index via the isothermal crystallization study.^{36,37} However, conventional DSC is not suitable for monitoring the fast initial crystallization process of the conjugated polymers due to the time mismatch between the slow scanning rate (up to 100 K/min) and the fast crystallization rate (over 1000 K/s). Only a few conjugated polymers with slow crystallization rates have been characterized by conventional DSC for such studies.^{33,38} Nevertheless, fast scanning calorimetry (FSC) has been demonstrated to be ideally suitable to probe the crystallization kinetics of conjugated polymers because of its ultrafast scanning rate (up to 10^6 K/s) enabled by the nanogram scale sample amount.^{12,34,39–42} The nonisothermal and isothermal crystallization kinetics of flexible poly(3-hexyl thiophene) (P3HT) have been investigated by FSC;^{34,41} however, rare work has reported the crystallization kinetics of donor–acceptor conjugated polymers, which typically give high charge-transport mobility, stability, and mechanical compliance.^{43–45} Unlike flexible polymers (e.g., P3HT), which typically crystallize in folded chain lamellae, extended chain crystallization occurs in most donor–acceptor conjugated polymers due to their planar, torsion-free backbone conformation.⁴⁶ With pre-existing structure history, flexible polymer chains grow into uniform folded chain lamellar crystals at the crystal growth front with accelerated crystallization kinetics.⁴⁷ The evolution of such extended chain crystals with pre-existing structure history might be different from that of folded chain crystals due to the different chain conformation, chain mobility, and interactions.

In this work, the crystallization behaviors of diketopyrrolopyrrole (DPP)-based donor–acceptor polymers are studied by FSC. Through the nonisothermal study, the critical cooling

rate (R_c) for the avoidance of crystalline formation was determined to be as fast as 200 000 K/s for dithienyl-diketopyrrolopyrrole (DPPT) and even over 500 000 K/s for DPP-based polymers with an increased size of fused thiophene rings. And, a two-step crystallization process was clearly extracted in DPP-based polymers by time-resolved FSC measurements. Using Avrami analysis, the increased rigidity of the chain backbones and the rapidly formed crystallites during the first-step crystallization process were found to accelerate the crystallization rate over an order of magnitude at the same degree of undercooling relative to the melting temperature. Based on these thermal characterizations, DPP-based polymer films with a higher crystallinity were obtained during thermal annealing by increased the preinduced aggregates which, in turn, leads to a higher charge transport mobility.

■ EXPERIMENTAL SECTION

Materials. The DPP-based conjugated polymers with systematically controlled backbone structures were synthesized via the reported methods.^{47–49} Their number-averaged molecular weights and polydispersity indexes were measured using high temperature gel permeation chromatography (calibrated with monodisperse polystyrene standards) performed at 170 °C with 1,2,4-trichlorobenzene as the solvent. The molecular weights and polydispersity indices of these polymers are shown in Table S1. Polymer solutions were first prepared in glass vials by dissolving 10 mg of sample in 1 mL of chloroform at 50 °C for 30 min. The ultrasonication-treated solution was prepared by ultrasonication of the solution for 5 min by an ultrasonic cleaner (35 kHz, 100W). The UV-treated solution was prepared by exposing the solution to UV irradiation (8 mW/cm², 254 nm) for 5 min. During the UV treatment, the vial was stirred at a speed of 300 rpm.

Thin Film Preparation. A thin layer of a water-soluble sacrificial layer (polystyrenesulfonate (PSS)) was first spin-coated on a cleaned silicon substrate. Next, conjugated polymer thin films were spin-coated on the PSS layer, obtaining a thickness around 80 nm. Then, thin films were annealed at 40 °C under vacuum for 30 min to remove the residual solvent and then cut into small pieces on the substrate. Finally, tiny pieces of conjugated polymer thin films were released by dipping the substrates into the water and transferred onto the heating area of XI-400 sensors.^{37,48} To control the mass of each sample, the film pieces were cut down to a size that just covered the heating area of the sensor as shown in Figure S7. The sensors were annealed under a vacuum at 40 °C for 2 h to remove residual water.

Fast Scanning Calorimetry. Crystallization studies of bulk samples were performed using the custom-made ultrafast FSC device in combination with XI-393 sensors (calibrated by indium).^{37,48} The XI-393 sensor has a work area of 6 μm × 8 μm. Thin layer samples were cut under the optical microscope by a sharp scalpel and then put on the center of the sensors' work area by a thin copper wire. Liquid nitrogen is used as a coolant here. All measurements were performed under an ambient nitrogen atmosphere. Unless otherwise specified, the cooling and heating rates of FSC used in this paper were 500 000 K/s and 100 000 K/s, respectively.

Flash DSC 1. Crystallization studies of thin film samples were performed using the Flash DSC 1 made by Mettler Toledo. An intracooler (TC100MT, Huber) enables the scanning temperature range between –90 and 450 °C and scanning rate up to 4000 K/s. The scanning rate of 4000 K/s was used in the measurements of thin film samples. Nitrogen was used as a purge gas with a constant flow of 20 mL/min. The MultiSTAR UFS1 (XI-400, Xensor Integrations, NL) based on MEMS (Micro-Electro-Mechanical Systems) technology was used as the chip sensors. The chip sensors were both conditioned and corrected for temperature calibration according to Mettler Toledo procedures before use.

Organic Field-Effect Transistor (OFET) Fabrication and Characterization. The electrical characterization was performed

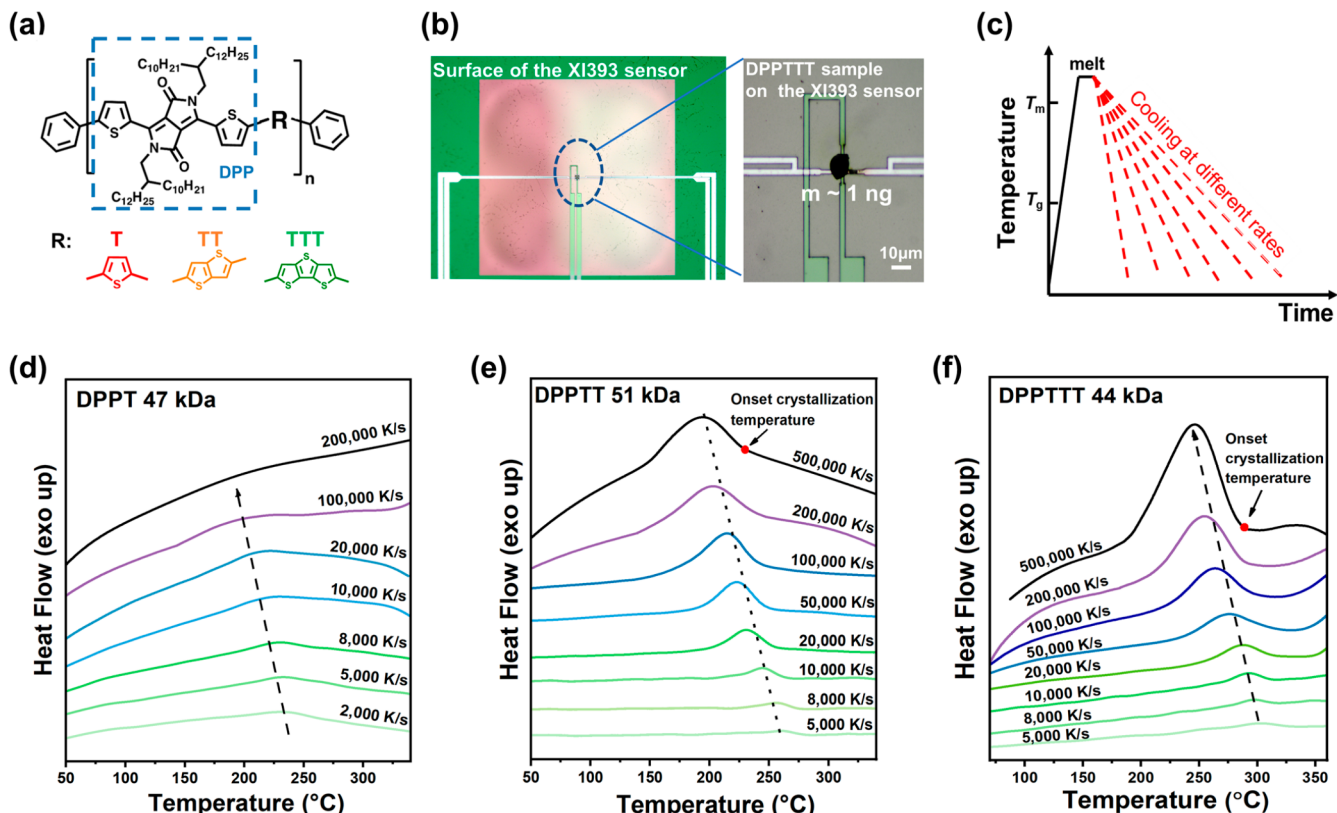


Figure 1. Nonisothermal crystallization behaviors in DPP-based conjugated polymers at different cooling rates. (a) Chemical structures of DPPT, DPPTT, and DPPTTT. (b) FSC sensors loaded with samples. (c) Temperature programs for the nonisothermal crystallization studies. (d–f) Cooling curves of FSC experiments for (d) DPPTT, (e) DPPTT, and (f) DPPTTT-44 kDa measured at different cooling rates.

on bottom-gate, bottom-contact field effect transistors fabricated by directly spin coating DPPTT films (1000 rpm for 60 s) on top of a rigid device stack (50 nm Au source and drain electrodes on OTS-treated 300 nm SiO₂/Si). The channel length (*L*) and width (*W*) are 200 μm and 4 mm, respectively. The capacitance of the dielectric layer is 11.5 nF cm⁻². All of the electrical characteristics of the semiconducting layer were measured using Keithley 4200 under an ambient environment. The drain current (*I*_{DS}) vs gate voltage (*V*_{GS}) was plotted. And, the charge carrier mobility was calculated in the regime between −80 V to 0 V by fitting the following equation:

$$I_{DS} = \frac{WC_{OX}}{2L} \mu (V_{GS} - V_t)^2$$

where *W* is the channel width, *L* is the channel length, *C_{ox}* is the capacitance per unit area of the dielectric layer, μ is the hole mobility, and *V_t* is the threshold voltage.

Morphological Characterizations. A Vecco nanoscope V atomic force microscope (AFM) was used to record the topography images of the thin films with different retreatment conditions and post-thermal annealing. Grazing incidence wide angle X-ray scattering (GIWAXS) experiments were performed using a lab-based Xuess 2.0 SAXS/WAXS instrument. The samples were measured with an X-ray wavelength of 1.54 Å for 5400 s at an incident angle of 0.2°. The scattering data was collected by a Pilatus 1 M detector with a sample-to-detector distance of 150 mm. Both 2D and 1D data were processed using Igor 8 software together with the Nika package and GIWAXS Tools. The relative degree of crystallinity was calculated through pole figure analysis on the 100 peak. The data was processed through background and geometry correction, followed by normalization of the film thickness and exposure time. Ultraviolet-visible absorption (UV-vis) spectra were obtained with a Shimadzu UV-3600 Plus UV-vis-NIR spectrophotometer.

RESULTS AND DISCUSSIONS

Ultrafast Crystallization Rate in DPP-Based Conjugated Polymers. The crystallization kinetics of DPP-based conjugated polymers with different sizes of fused thiophene rings (Figure 1a and Table S1, Supporting Information) are first investigated here by nonisothermal crystallization studies. The exotherms of DPP-based conjugated polymers at different cooling rates are presented in Figure 1. Due to the tiny sampling amount on the chip sensor (8 μm × 14 μm, Figure 1b), a well-controlled scanning rate up to 500 000 K/s can be achieved by FSC.

In these nonisothermal crystallization experiments (Figure 1c–f), the polymer samples were first heated above the melting temperatures (*T_m*) and held for 0.1 s to melt out any existing crystals. Next, the samples were cooled down at different cooling rates to their glassy state, and the cooling curves were recorded by FSC. If the sample is cooled at a rate faster than needed for forming crystals, the crystallization can be suppressed. The critical cooling rate (*R_c*) here can be used to qualitatively compare the crystallization kinetics in materials. As shown in Figure 1d, the crystallization peak in the cooling curves of DPPT disappeared at a cooling rate of 200 000 K/s, indicating the *R_c* of DPPT is reached. Compared with the reported *R_c* (30 000 K/s) of P3HT,^{41,49} *R_c* of DPPT is much higher, implying much faster crystallization kinetics in DPPT. With the further increase of the size of the thiophene unit, the crystallization of thieno[3,2-*b*]thiophene-diketopyrrolopyrrole (DPPTT) and dithieno[3,2-*b*:3',2'-*d*]thiophene-diketopyrrolopyrrole (DPPTTT-44 kDa) during cooling could not be avoided even at the cooling rate up to 500 000 K/s (Figure

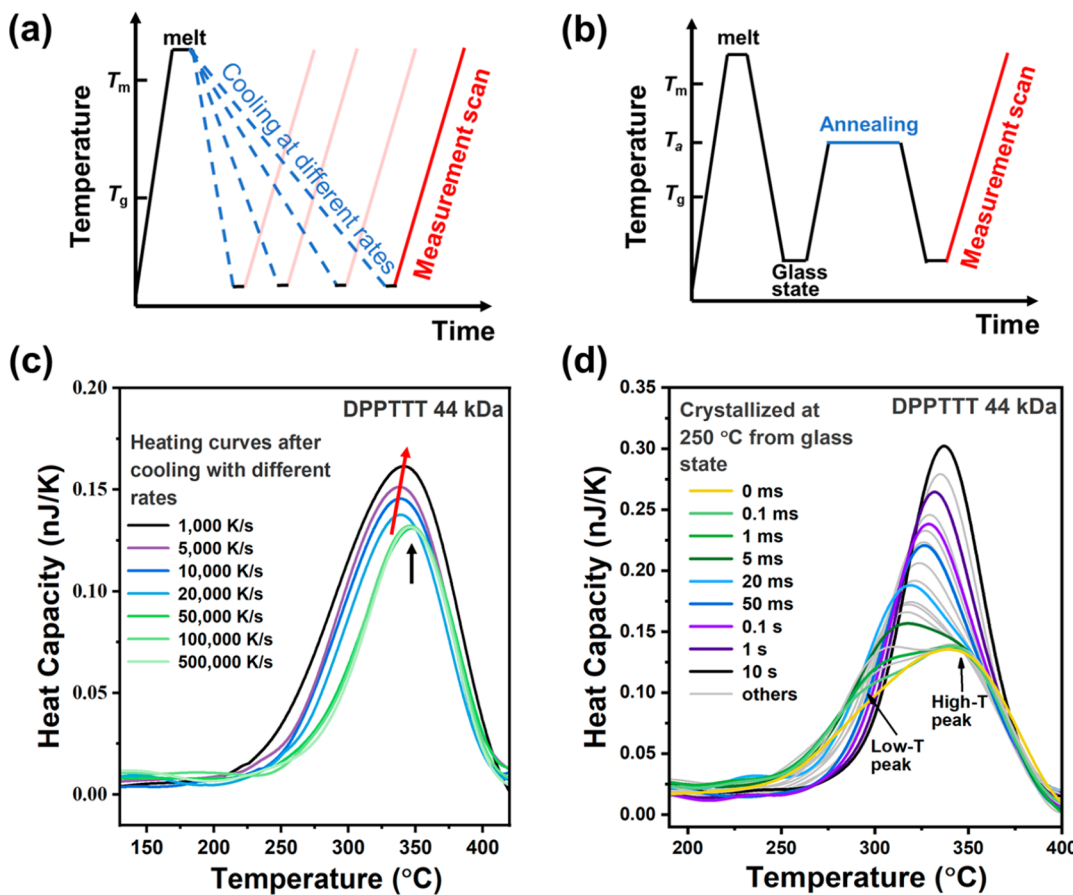


Figure 2. Two-step crystallization process observed in DPPTT. (a, b) Temperature programs for the studies of nonisothermal crystallization (a) and isothermal crystallization (b). (c) Heating curves of FSC experiments after cooling with different rates and holding at $-100\text{ }^{\circ}\text{C}$ for 0.5 s for the DPPTT-44 kDa sample. (d) Reheating curves of FSC experiments after isothermal crystallization at $250\text{ }^{\circ}\text{C}$ for the DPPTT-44 kDa sample. The heating rate and cooling rates (except for the blue lines in (a)) are $100\,000\text{ K/s}$ and $500\,000\text{ K/s}$, respectively. The black arrow and red arrow in (c) indicate the crystals formed at the first-step crystallization and the crystals stabilized during the second-step crystallization, respectively.

1e,f), which is close to the predicted R_c of high-density polyethylene with extremely fast crystallization.⁵⁰ Even though these DPP-based polymers contain bulky side groups, we infer that their rod-like rigid backbone structures and strong intermolecular forces resulted from the $\pi-\pi$ interactions among chromophores strongly drive the polymer segments to crystallize at an ultrafast rate. With the further increase of the backbone rigidity by introducing a larger fused thiophene unit,⁷ even faster nonisothermal crystallization kinetics is enabled.

Two-Step Crystallization Process in DPP-Based Polymers. To further explore the evolution of the crystallization process in DPP-based polymers during cooling, we performed two types of thermal characterizations by FSC. First, the nonisothermal crystallization process of the DPPTTT and DPPTT polymers was studied by a cooling-rate-dependent characterization using the temperature program illustrated in Figure 2a. As shown in Figure 2c and Figure S1, the melting peak can be observed in each heating curve after cooling with rates ranging from 1000 K/s to $500\,000\text{ K/s}$. We note that the melting peaks overlap in the heating curves after cooling at rates from $500\,000\text{ K/s}$ to $50\,000\text{ K/s}$ for both DPPTT and DPPTTT samples (as pointed to by the black arrow in Figure 2c), indicating a constant amount of crystals formed during these thermal processes. When the cooling rate is lower than $20\,000\text{ K/s}$, the melting peak starts to increase. This

phenomenon implies a two-step crystallization behavior in these DPP-based polymers, including an ultrafast crystallization (first-step) accomplished during the cooling at rates even higher than $500\,000\text{ K/s}$, and then a relatively slower crystallization (second-step) starts to occur at cooling at rates lower than $20\,000\text{ K/s}$. The second-step starts to occur at cooling at rates lower than $20\,000\text{ K/s}$. The increased T_m indicates the increased extended length of the chains in the crystalline fraction and the perfection of crystalline structure to higher stability.⁵¹ Here, the T_m values of the rapidly formed crystallites during the first step exhibit a high value, suggesting a stable crystalline structure already formed. With further decreasing the cooling rates, the T_m value first decreases and then gradually increases with the melting peaks getting broader and bigger (red arrow in Figure 2c), indicating the crystallites that formed during the second step gradually grow and stabilize.

To confirm this hypothesis of two-step crystallization, second, we performed the isothermal crystallization study on DPP-based samples through the temperature program shown in Figure 2b. Samples were first heated to melt and then quenched at $500\,000\text{ K/s}$ to $-100\text{ }^{\circ}\text{C}$. Then, the samples were heated up again ($100\,000\text{ K/s}$) to a desired isothermal temperature and left crystallized for a certain length of time and then quenched ($500\,000\text{ K/s}$) to $-100\text{ }^{\circ}\text{C}$. At last, the growth of crystals during the previous isothermal process was

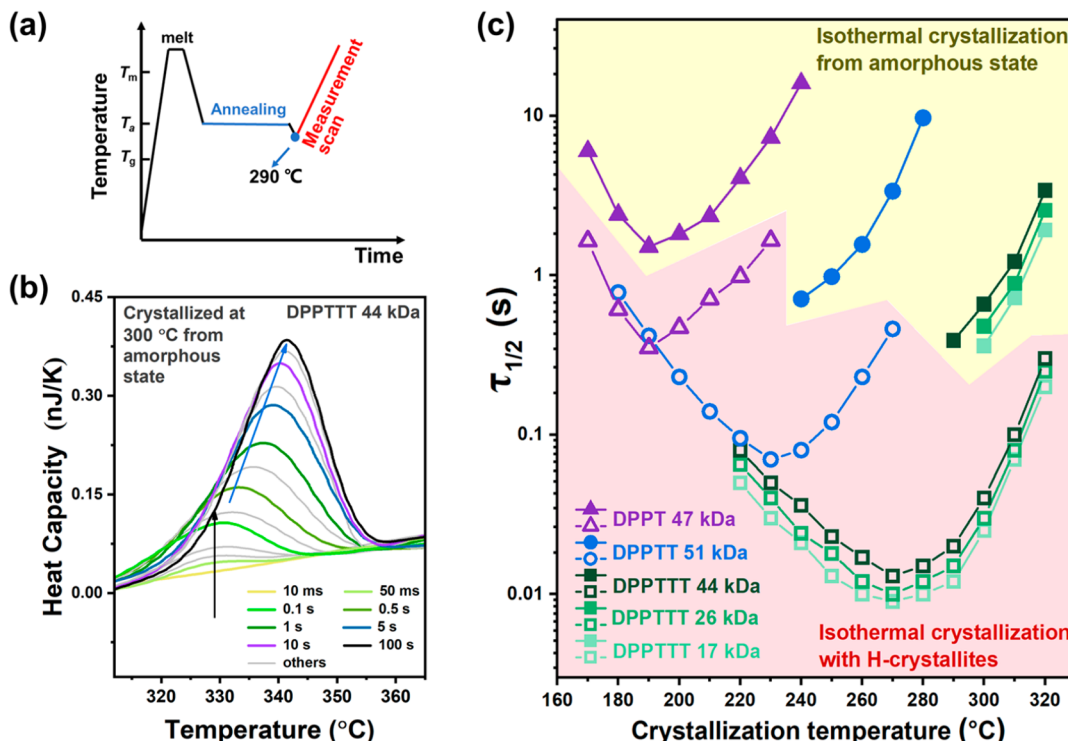


Figure 3. Accelerated crystallization kinetics in DPP-based polymers with preformed H-crystallites. (a) Time–temperature program of the experiments for the study of isothermal crystallization from the amorphous state. (b) Reheating after isothermal crystallization from the amorphous state at 300 °C of the DPPTT-44 kDa sample. (c) Crystallization half-time of DPPT, DPPTT, and DPPTTT samples as a function of the crystallization temperature. The solid symbols indicate the isothermal crystallization from the amorphous state. The hollow samples indicate the isothermal crystallization after the formation of H-crystallites. Detailed crystallization kinetics of each sample are shown in Figures S6 and S7.

monitored quantitatively by analyzing the melting peaks in the last heating scan curves. This isothermal crystallization was investigated at a wide range of temperatures, which will be discussed in the next section. Figure 2d shows the isothermal crystallization of the DPPTT-44 kDa sample at 250 °C as an example to illustrate the details. Two melting peaks (marked as high- T and low- T) were clearly observed in the heating curves with the high- T peak remaining the same within the first few milliseconds of isothermal crystallization. This confirms the existence of the two-step crystallization process we observed in the nonisothermal study, and this high- T peak corresponds to the melting of the crystallites formed during quenching at a high crystallization rate (H-crystallites). During annealing, second step crystallizations occurred, as determined by the increased temperature and area of the low- T peak. Eventually, the low- T and high- T peaks gradually merge into one peak, moving slowly toward higher temperatures because of the formation of larger crystallites with a higher thermal stability during annealing. Surprisingly, the melting temperature (the merged peak) of crystals in the sample annealed for 10 s is still lower than that (initial high- T peak) of H-crystallites formed during quenching. This result indicates the higher stability of crystallites formed at first step crystallization during quenching. Similar results were also observed for DPPTT and DPPTTT samples with different M_w values as shown in Figure S2. Such rod-like rigid backbone structures and the strong intermolecular forces resulting from the π – π interactions strongly drive the D–A polymer segments to form locally ordered structures at an ultrafast rate from melt or concentrated solutions, which is the origin of the H-crystallite formation. After the formation of these initial H-crystallites, the average

dynamic mobility of conjugated polymer chains in the amorphous region decreases due to the restrictions from the formation of the rigid amorphous region near the crystalline regions.^{48,52,53} Such suppressed segmental mobility reduces chances for chain segments to further form ordered crystal nuclei and incorporate additional available segments onto the established crystals. The system needs to absorb more energy to overcome the potential energy barrier for further crystallization. As the crystallinity of this DPP-based conjugated polymer is low,¹⁰ most of the conjugated polymer chains are still in the amorphous regions. When giving more thermal energy (by reducing cooling rate or annealing), the conjugated polymer chains which are “far away” from the H-crystalline regions move first as they have relatively higher dynamic mobility than the ones near the H-crystalline regions and form the new/secondary local ordered structures (i.e., primary crystallization of the second-step crystallization process). Thus, we observed such two crystallization steps in the rigid D–A copolymers.

Two Types of Isothermal Crystallization Kinetics in DPP-Based Polymers with or without H-Crystallites. The crystallization kinetics of polymeric materials relies on many factors, including chain rigidity, molecular weight, and pre-existing microstructures.^{21,33} Isothermal crystallization studies have been demonstrated as a powerful method for analyzing the crystallization kinetics of polymers.^{36,37} However, such studies for conjugated polymers are challenging because their strong tendency to crystallize makes it difficult to reach a truly amorphous state in which controlled annealing can be carried out. In this work, two types of isothermal crystallization studies were designed and compared, which involve (1) rapid

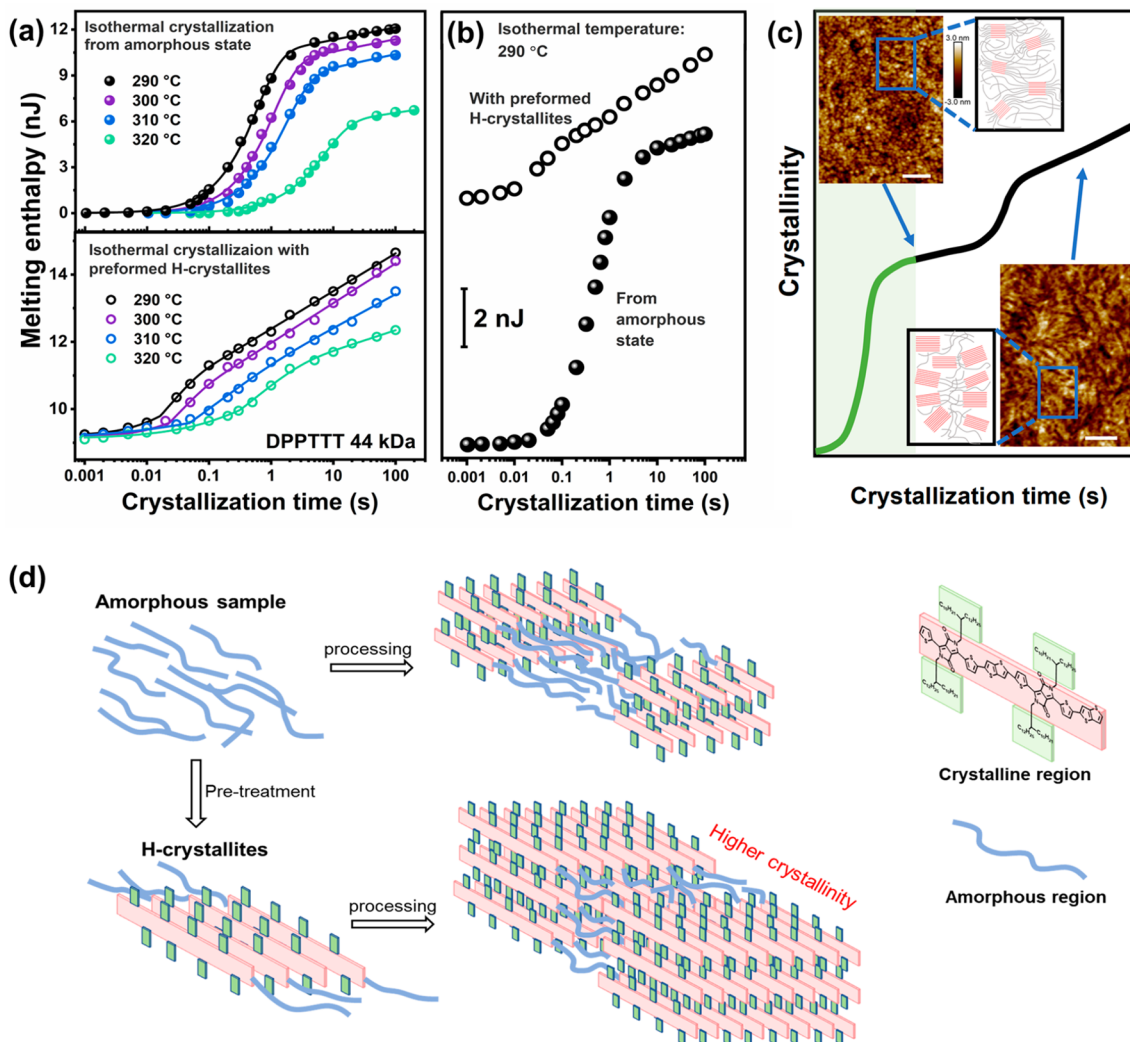


Figure 4. Promoted crystal growth of DPPTTT-44 kDa with preformed H-crystallites. (a) Melting enthalpies of isothermal crystallization of DPPTTT-44 kDa from the amorphous state (top) and with preformed H-crystallites (bottom) as a function of the crystallization time. Data points were fitted using a modified Kolmogorov–Johnson–Mehl–Avrami equation.³⁶ (b) Melting enthalpies of the isothermal crystallization of DPPTTT-44 kDa at 290 °C with and without H-crystallites. (c) Illustration of the two-step crystallization mechanism of commonly processed DPP-based polymers. The green curve indicates the crystal formation at the first step, while the black curve indicates the crystal formation with slower kinetics. Inset AFM images indicate the morphologies of the samples quenched from the melt and after a long time of annealing, respectively. The scale bar indicates 200 nm. (d) Schematic image of the impact of the presence of preformed H-crystallites on the isothermal crystallization.

quenching from melt to an annealing temperature that was set higher than the onset temperature of crystallization to avoid the nonisothermal crystallization (**Figure 3a**) and (2) rapid quenching from the melt to glass, followed by controlled annealing at different temperatures (**Figure 2b**). According to the thermogravimetric analysis (TGA) (**Figure S3**) and thermal cycling study (**Figure S4**), fast scanning permits exposing the sample at high temperatures for a time shorter than that necessary to start degradation.

The first type of isothermal crystallization allows the study of the crystallization kinetics of DPP-based conjugated polymers crystallizing from the amorphous state. For DPPTT and DPPTTT samples, the crystallizations during cooling start at the temperatures of 230 and 290 °C (**Figure 1e,f**), respectively. In order to avoid any crystallizations during cooling, the temperatures of the isothermal annealing and the onset of measurement were set above 230 and 290 °C for DPPTT and

DPPTTT samples, respectively. As the crystallization of DPPT can be fully suppressed at the cooling speed of 500 000 K/s, the range of the annealing temperatures was set broader. **Figure 3b** plots the heating curves of the DPPTTT-44 kDa polymer crystallized at 300 °C for different lengths of time as an example to show the details of crystal growth. From the heating curves, we found that there was nearly no crystal formed after the polymers were annealed for 10 ms (yellow curve). During the annealing time between 50 and 100 ms, the melting peak position is almost constant with an increasing peak area, indicating the formation of primary crystals (black arrow in **Figure 3b**).³⁶ After 100 ms, the T_m value kept increasing with the increased annealing time, implying the further growth and stabilizing of the crystals (blue arrow in **Figure 3b**). Similar results were observed in DPPT and DPPTT samples (**Figure S5**). The areas of the melting peak as a function of the crystallization time were plotted for each

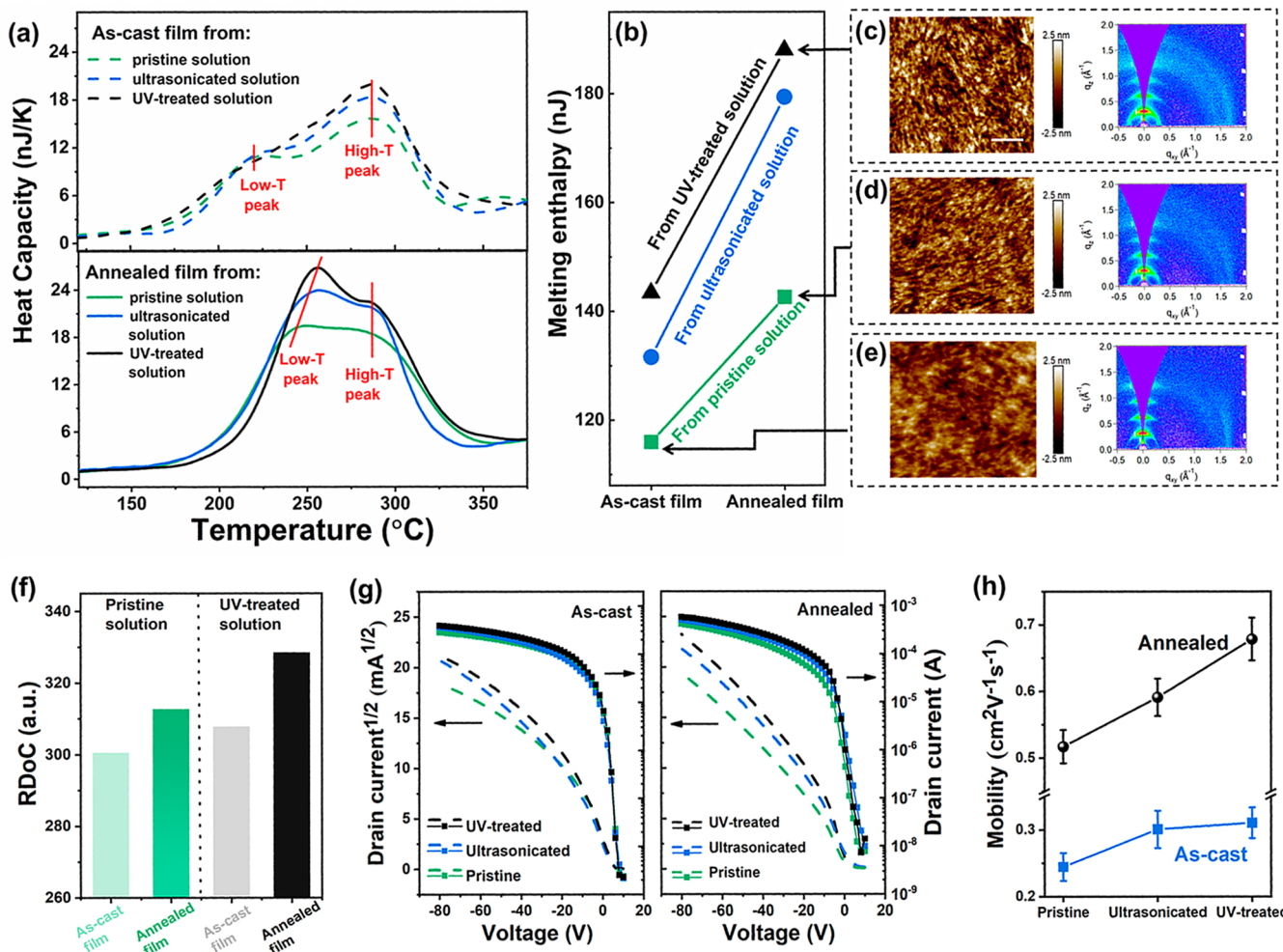


Figure 5. (a) Heating scans of as-cast films (top) and annealed films (bottom) deposited via spin-coating from pristine solution, ultrasonicated solution, and UV-treated solution. (b) Melting enthalpies of as-cast films and annealed films deposited via spin-coating from pristine solution, ultrasonicated solution, and UV-treated solution. The annealing process was performed at 170 °C for 10 min. AFM images and 2D GIWAXS patterns for the (c) annealed film from the UV-treated solution, (d) annealed film from the pristine solution, and (e) as-cast film from the pristine solution. The scale bar indicates 200 nm. (f) Relative degree of crystallinity (RDoC) of as-cast and annealed films spin-coated from pristine and UV-treated solutions determined by 2D GIWAXS. (g) Characteristic transfer curves and (h) calculated mobilities of films through different pre- and post-treatments.

sample (Figure S6), which allowed the determination of the crystallization half-time through the modified Avrami equation,^{36,54} considering primary and secondary crystallization:

$$\Delta H = \Delta H_{\infty} \left\{ 1 - \exp \left[- \left(\frac{t}{\tau_{1/2}} \ln 2 \right)^n \right] \right\} + A_2 (\ln t - \ln \tau_{1/2}) \left[\frac{1}{2} \left(\frac{|t - \tau_{1/2}|}{t - \tau_{1/2}} + 1 \right) \right] \quad (1)$$

Here, ΔH is the total enthalpy change measured on heating, ΔH_{∞} is the enthalpy change of primary crystallization, t is the crystallization time, $\tau_{1/2}$ is the crystallization half-time, n represents the Avrami coefficient, and A_2 is a secondary crystallization parameter. The half times of the first type of isothermal crystallization are shown in the yellow region (solid symbols) of Figure 3c.

The second type of isothermal crystallization studies the crystallization kinetics of DPP-based conjugated polymers with pre-existing H-crystallites (formed during quenching). As

discussed above, after the cooling from the melt to glass state at a rate of 500 000 k/s for DPPTT and DPPTTT, some crystallites with high stabilities can be formed. A rate of 50 000 K/s is chosen for the DPPT sample to enable the formation of H-crystallites in its initial microstructure. Following the temperature program illustrated in Figure 2b, heating scans after the isothermal crystallization of DPP-based polymers were measured by FSC. Equation 1 was used to plot the melting-peak areas as a function of crystallization time as shown in Figure S7.

Figure 3c summarizes the calculated crystallization half times to demonstrate the isothermal crystallization kinetics of DPP-based polymers with different backbone rigidities and different M_w values, as well as with or without preformed H-crystallites. Most interestingly, $\tau_{1/2}$ of the DPP polymers with the presence of preformed H-crystallites could be more than 1 order of magnitude shorter than the one crystallized from the amorphous state. This indicates that the presence of H-crystallites can significantly accelerate the crystal growth during annealing. Second, with the same thermal history, the isothermal crystallization behaviors strongly correlate with

the backbone structure. With the increased size of the fused thiophene unit in the conjugated backbone, the highest crystallization rate (lowest $\tau_{1/2}$) for each sample and the temperature to reach this rate both increased. Compared to the pre-existing crystallites and chain rigidity, M_w exhibits much less influence on the crystallization kinetics in DPPTT polymers.

The influence of the preformed H-crystallites on the crystal growth of DPPTT in the previous two types of isothermal crystallization was further studied in Figure 4. The melting enthalpies of DPPTT that underwent the two types of isothermal crystallization at temperatures from 290 to 320 °C were plotted as a function of the crystallization time in Figure 4a. We found that the overall crystallinity in DPPTT with preformed H-crystallites was higher than that of the sample crystallized from the amorphous state during the same annealing condition (Figure 4b). Combining the two curves of the crystal growth here with the above studies, a schematic image of the two-step crystallization process that may exist in most commonly processed DPP-based conjugated polymers was illustrated in Figure 4c, including an extremely fast first-step crystallization ($\sim\mu\text{s}$) and a relatively slower second-step crystallization. From the AFM images, the sample quenched from melt to glass exhibits a morphology with a lot of nodular domains while more fibril structures were observed in the annealed sample, indicating the further crystal development that connected nodular domains during second-step crystallization.

The impact of H-crystallites on the subsequent crystallization is demonstrated by the schematic image in Figure 4d. Unlike flexible polymers (e.g., P3HT), which typically crystallize in folded chain lamellae, rigid and highly planar D–A polymer chains without folding tend to grow into the extended chain crystals. The relatively planar backbone structures and the strong intermolecular forces strongly drive the D–A polymer segments to form into H-crystallites when they are cooled from the melt at an ultrafast rate. Then new crystals could grow easier on the surface of the existing H-crystallites during processing due to low surface free energy, leading to a higher crystallization rate and promoted crystallinity than that from the amorphous state. These observations indicate a higher degree of crystallinity can be achieved by processing, which could further impart the electrical property in these DPP-based conjugated polymers.

Promoted Crystallizations Enable Higher Charge Carrier Mobilities. The above studies of crystallization behaviors by FSC can provide the knowledge of designing processing protocols for DPP-based polymers to achieve more crystallized microstructures, which are favorable for the electrical performance. Usually, these DPP-based conjugated polymers are solution-processed into thin films and then thermally annealed at a temperature below the melting point for further crystallization before being fabricated into devices. Based on the observations in Figures 3 and 4, we infer that the boosting of preformed aggregates (nanocrystalline) in solutions may enhance the first step crystallization during solidification (solution-processing) and further improve the crystal growth during the follow-up thermal processing in DPP-based polymer films. Using morphological characterization methods, people have observed the improved crystallization in P3HT films by introducing aggregations in P3HT solutions through ultrasonication and low-dose UV irradiation.^{21,25,55,56} Here, we explored the impact of such

preformed H-crystallites on the crystallization behaviors in DPP-based polymers using thermal characterizations enabled by FSC.

DPPTT polymer solutions were first pretreated by ultrasonication or UV irradiation to promote the growth of aggregates in solutions (Figure S8). Then, three types of thin films were spin-coated from these two treated solutions and one untreated solution (control), respectively. These prepared films were transferred to the Flash DSC sensor with a larger sensing area for better signal resolution (Figure S9). From Figure 5a, two-step crystallization behavior was again found during polymer solidification from solutions as indicated by the two melting peaks in the first heating curves of these three as-cast films. We note here that the difference of the melting temperature (T_m) of each peak between the film sample and the bulk sample could be caused by the restricted growth of crystals under a nanoconfinement effect.⁵⁷ A larger area of the high- T peak was observed in the curves of the films spin-coated from pretreated solutions, which indicates that the increased preformed aggregations in solutions can promote the first-step crystallization during solidification. Even though FSC can detect the crystals with the size down to a few nanometers, the low T_m peak corresponds to the melting of different types of crystallite from that of the high- T peak rather than the melting of aggregates in the sample. After annealing at 170 °C for 10 min (Figure 5b), the total melting enthalpies increased considerably in all three films, with more increments in the films spin-coated from pretreated solutions than untreated solutions as implied by the steeper slopes shown in Figure 5c. In addition, after post-thermal treatment, the melting temperatures (low- T peak) of the films spin-coated from pretreated solutions were higher than that of the film spin-coated from the pristine solution, indicating thicker lamellas with higher thermal stability were formed in the films spin-coated from pretreated solutions during the annealing process. These thermal characterizations clearly show the two-step crystallization mechanism in DPPTT polymers and the promoted crystallization during subsequent annealing by introducing preformed H-crystallites in the as-cast films. Compared with the as-casted and annealed films deposited from the untreated solution, the corresponding ones prepared from pretreated solutions showed more obvious fibril-like morphologies and slight increments of surface roughness (0.55 nm for Figure 5c, 0.77 nm for Figure 5d, and 0.92 nm for Figure 5e) from AFM images, indicating more crystalline structures (Figure 5c–e, left, and Figure S10). GIWAXS measurements showed that the relative degree of crystallinity (RDoC) of the films spin-coated from UV-treated solution was higher than that of films spin-coated from the pristine solution (Figure 5c–e, right, Figure 5f, and Figure S11).^{7,58} These morphological characterizations are consistent with the observations from the thermal characterizations.

The charge-carrier mobility of these DPPTT films was measured in thin-film transistors with a bottom-gate–bottom-contact device structure. As shown in Figure 5g,h and Figure S12, the as-cast DPPTT films prepared from pretreated solutions display higher currents (I_D) and charge carrier mobilities (μ) than those of the as-casted film prepared from the untreated solution. When these films were annealed at 170 °C for 10 min, I_D and μ of the annealed films were all increased, with more increases observed in the annealed films prepared from pretreated solutions. These electrical characterizations again confirm the results from the thermal studies and

demonstrate how knowledge gained from thermal studies play a role in designing the processing protocol for achieving better performance.

CONCLUSIONS

In summary, FSC was employed to reveal the crystallization behaviors of DPP-based conjugated polymers with different chain rigidities, molecular weights, and pre-existing microstructures at scanning rates up to 500 000 K/s. Through elaborately designed nonisothermal and isothermal crystallization studies, we probed the ultrafast crystallization kinetics and extracted a two-step crystallization process in these polymers quantitatively. The crystallites formed in the first step display an extremely fast crystallization rate and high thermal stability. Based on these thermal characterizations, we found that both the rigidity of the chain backbones and the pre-existing crystalline microstructures can influence the crystallization rate over an order of magnitude at the same degree of undercooling relative to the melting temperature. We further demonstrated the manipulated crystallization kinetics in the DPP-based polymer films with different amounts of preinduced crystallites and correlate it to the polymers' charge transport mobility. These time-resolved thermal analyses of the crystallization behaviors of these DPP-based conjugated polymers provide insights into how the polymer chemical structure and pre-existing microstructure influence the crystallization kinetics, which, in turn, could provide guidance on the design rules for conjugated polymer structures and process conditions for better control of the final active layer microstructures in polymer-based electronics.

ASSOCIATED CONTENT

Supporting Information

The Supporting Information is available free of charge at <https://pubs.acs.org/doi/10.1021/acs.chemmater.0c03854>.

Physical properties of DPP polymers used in the study; thermogravimetric analysis (TGA) data; additional FSC data; UV-vis absorption spectra of the polymer solution; thin film sample image on the Flash DSC sensor; additional AFM images; and additional device data ([PDF](#))

AUTHOR INFORMATION

Corresponding Authors

Jie Xu — Nanoscience and Technology Division, Argonne National Laboratory, Lemont, Illinois 60439, United States; [ORCID iD](https://orcid.org/0000-0001-7842-5496); Email: xuj@anl.gov

Dongshan Zhou — Department of Polymer Science and Engineering, School of Chemistry and Chemical Engineering, Shenzhen R&D Center, State Key Laboratory of Coordination Chemistry, Key Laboratory of High Performance Polymer Materials and Technology MOE, Nanjing University, Nanjing 210023, P. R. China; [ORCID iD](https://orcid.org/0000-0002-0038-7589); Email: dzhou@nju.edu.cn

Chao Teng — Institute of Marine Biomedicine, Shenzhen Polytechnic, Shenzhen 518055, China; Email: tengchao@szpt.edu.cn

Authors

Shaochuan Luo — Department of Polymer Science and Engineering, School of Chemistry and Chemical Engineering,

Shenzhen R&D Center, State Key Laboratory of Coordination Chemistry, Key Laboratory of High Performance Polymer Materials and Technology MOE, Nanjing University, Nanjing 210023, P. R. China; Pritzker School of Molecular Engineering, University of Chicago, Chicago, Illinois 60637, United States

Nan Li — Pritzker School of Molecular Engineering, University of Chicago, Chicago, Illinois 60637, United States

Song Zhang — School of Polymer Science and Engineering, Center for Optoelectronic Materials and Devices, University of Southern Mississippi, Hattiesburg, Mississippi 39406, United States; [ORCID iD](https://orcid.org/0000-0001-9815-7046)

Chen Zhang — Institute of Marine Biomedicine, Shenzhen Polytechnic, Shenzhen 518055, China

Tengfei Qu — Department of Polymer Science and Engineering, School of Chemistry and Chemical Engineering, Shenzhen R&D Center, State Key Laboratory of Coordination Chemistry, Key Laboratory of High Performance Polymer Materials and Technology MOE, Nanjing University, Nanjing 210023, P. R. China

Michael U. Ocheje — Department of Chemistry and Biochemistry, University of Windsor, Windsor, Ontario N9B3P4, Canada

Gi Xue — Department of Polymer Science and Engineering, School of Chemistry and Chemical Engineering, Shenzhen R&D Center, State Key Laboratory of Coordination Chemistry, Key Laboratory of High Performance Polymer Materials and Technology MOE, Nanjing University, Nanjing 210023, P. R. China

Xiaodan Gu — School of Polymer Science and Engineering, Center for Optoelectronic Materials and Devices, University of Southern Mississippi, Hattiesburg, Mississippi 39406, United States; [ORCID iD](https://orcid.org/0000-0002-1123-3673)

Simon Rondeau-Gagné — Department of Chemistry and Biochemistry, University of Windsor, Windsor, Ontario N9B3P4, Canada; [ORCID iD](https://orcid.org/0000-0003-0487-1092)

Wenbing Hu — Department of Polymer Science and Engineering, School of Chemistry and Chemical Engineering, Shenzhen R&D Center, State Key Laboratory of Coordination Chemistry, Key Laboratory of High Performance Polymer Materials and Technology MOE, Nanjing University, Nanjing 210023, P. R. China; [ORCID iD](https://orcid.org/0000-0002-7795-9004)

Sihong Wang — Pritzker School of Molecular Engineering, University of Chicago, Chicago, Illinois 60637, United States

Complete contact information is available at:

<https://pubs.acs.org/10.1021/acs.chemmater.0c03854>

Notes

The authors declare no competing financial interest.

ACKNOWLEDGMENTS

S.L., D.Z., C.T., and J.X. conceived and designed the experiments. S.L., D.Z., and C.T. are grateful for the support from the National Natural Science Foundation of China (No. 21790345, 51673094), Guangdong Basic and Applied Basic Research Foundation (2019A1515110647), and Shenzhen Science and Technology Innovation Committee (JCYJ20170818110206085, JCYJ20170818110613113, JCYJ20200109141808025, GJHZ20190819151807167). J.X. acknowledges the Center for Nanoscale Materials, a U.S. Department of Energy Office of Science User Facility, and is

supported by the U.S. Department of Energy, Office of Science, under Contract No. DE-AC02-06CH11357. N.L. and S.W. thank the start-up support from the University of Chicago. S.Z. and X.G. are grateful for the financial support from U.S. Department of Energy, Office of Science, Office of Basic Energy Science, under Award Number DE-SC0019361 to assisting the scattering experiment in this work. C.Z. thanks the National Natural Science Foundation of China (No.21803004). S.R.-G. would like to thank the Natural Science and Engineering Research Council of Canada (NSERC) for financial support through a Discovery Grant (RGPIN-2017-06611) and the Canadian Foundation for Innovation (CFI). M.U.O. thanks NSERC for a postgraduate doctoral scholarship.

■ REFERENCES

- (1) Xu, J.; Wang, S.; Wang, G.-J. N.; Zhu, C.; Luo, S.; Jin, L.; Gu, X.; Chen, S.; Feig, V. R.; To, J. W. F.; Rondeau-Gagne, S.; Park, J.; Schroeder, B. C.; Lu, C.; Oh, J. Y.; Wang, Y.; Kim, Y.-H.; Yan, H.; Sinclair, R.; Zhou, D.; Xue, G.; Murmann, B.; Linder, C.; Cai, W.; Tok, J. B. H.; Chung, J. W.; Bao, Z. Highly stretchable polymer semiconductor films through the nanoconfinement effect. *Science* **2017**, *355* (6320), 59–64.
- (2) Cheng, P.; Li, G.; Zhan, X. W.; Yang, Y. Next-generation organic photovoltaics based on non-fullerene acceptors. *Nat. Photonics* **2018**, *12* (3), 131–142.
- (3) Wang, S. H.; Xu, J.; Wang, W. C.; Wang, G. J. N.; Rastak, R.; Molina-Lopez, F.; Chung, J. W.; Niu, S. M.; Feig, V. R.; Lopez, J.; Lei, T.; Kwon, S. K.; Kim, Y.; Foudeh, A. M.; Ehrlich, A.; Gasperini, A.; Yun, Y.; Murmann, B.; Tok, J. B. H.; Bao, Z. A. Skin electronics from scalable fabrication of an intrinsically stretchable transistor array. *Nature* **2018**, *555* (7694), 83–88.
- (4) Zhang, S.; Cheng, Y.-H.; Galuska, L.; Roy, A.; Lorenz, M.; Chen, B.; Luo, S.; Li, Y.-T.; Hung, C.-C.; Qian, Z.; St. Onge, P. B. J.; Mason, G. T.; Cowen, L.; Zhou, D.; Nazarenko, S. I.; Storey, R. F.; Schroeder, B. C.; Rondeau-Gagné, S.; Chiu, Y.-C.; Gu, X. Tacky Elastomers to Enable Tear-Resistant and Autonomous Self-Healing Semiconductor Composites. *Adv. Funct. Mater.* **2020**, *30* (27), 2000663.
- (5) Kim, M.; Ryu, S. U.; Park, S. A.; Choi, K.; Kim, T.; Chung, D.; Park, T. Donor-Acceptor-Conjugated Polymer for High-Performance Organic Field-Effect Transistors: A Progress Report. *Adv. Funct. Mater.* **2020**, *30* (20), 1904545.
- (6) Cao, Z.; Galuska, L.; Qian, Z.; Zhang, S.; Huang, L.; Prine, N.; Li, T.; He, Y.; Hong, K.; Gu, X. The effect of side-chain branch position on the thermal properties of poly (3-alkylthiophenes). *Polym. Chem.* **2020**, *11* (2), S17–S26.
- (7) Zhang, S.; Ocheje, M. U.; Huang, L.; Galuska, L.; Cao, Z.; Luo, S.; Cheng, Y.-H.; Ehlenberg, D.; Goodman, R. B.; Zhou, D.; Liu, Y.; Chiu, Y.-C.; Azoulay, J. D.; Rondeau-Gagné, S.; Gu, X. The Critical Role of Electron-Donating Thiophene Groups on the Mechanical and Thermal Properties of Donor-Acceptor Semiconducting Polymers. *Advanced Electronic Materials* **2019**, *5* (5), 1800899.
- (8) Zhang, S.; Ocheje, M. U.; Luo, S.; Ehlenberg, D.; Appleby, B.; Weller, D.; Zhou, D.; Rondeau-Gagné, S.; Gu, X. Probing the Viscoelastic Property of Pseudo Free-Standing Conjugated Polymeric Thin Films. *Macromol. Rapid Commun.* **2018**, *39* (14), 1800092.
- (9) Xu, J.; Wu, H.-C.; Zhu, C.; Ehrlich, A.; Shaw, L.; Nikolka, M.; Wang, S.; Molina-Lopez, F.; Gu, X.; Luo, S.; Zhou, D.; Kim, Y.-H.; Wang, G.-J. N.; Gu, K.; Feig, V. R.; Chen, S.; Kim, Y.; Katsumata, T.; Zheng, Y.-Q.; Yan, H.; Chung, J. W.; Lopez, J.; Murmann, B.; Bao, Z. Multi-scale ordering in highly stretchable polymer semiconducting films. *Nat. Mater.* **2019**, *18* (6), 594.
- (10) Noriega, R.; Rivnay, J.; Vandewal, K.; Koch, F. P.; Stingelin, N.; Smith, P.; Toney, M. F.; Salleo, A. A general relationship between disorder, aggregation and charge transport in conjugated polymers. *Nat. Mater.* **2013**, *12* (11), 1038–44.
- (11) Fratini, S.; Nikolka, M.; Salleo, A.; Schweicher, G.; Sirringhaus, H. Charge transport in high-mobility conjugated polymers and molecular semiconductors. *Nat. Mater.* **2020**, *19* (5), 491–502.
- (12) Luzio, A.; Nübling, F.; Martin, J.; Fazzi, D.; Selter, P.; Gann, E.; McNeill, C. R.; Brinkmann, M.; Hansen, M. R.; Stingelin, N. Microstructural control suppresses thermal activation of electron transport at room temperature in polymer transistors. *Nat. Commun.* **2019**, *10* (1), 3365.
- (13) Persson, N. E.; Chu, P. H.; McBride, M.; Grover, M.; Reichmanis, E. Nucleation, Growth, and Alignment of Poly(3-hexylthiophene) Nanofibers for High-Performance OFETs. *Acc. Chem. Res.* **2017**, *50* (4), 932–942.
- (14) Tanaka, H.; Wakamatsu, A.; Kondo, M.; Kawamura, S.; Kuroda, S.-i.; Shimoi, Y.; Park, W.-T.; Noh, Y.-Y.; Takenobu, T. Microscopic observation of efficient charge transport processes across domain boundaries in donor-acceptor-type conjugated polymers. *Communications Physics* **2019**, *2* (1), 96.
- (15) Boudouris, B. W.; Ho, V.; Jimison, L. H.; Toney, M. F.; Salleo, A.; Segalman, R. A. Real-Time Observation of Poly(3-alkylthiophene) Crystallization and Correlation with Transient Optoelectronic Properties. *Macromolecules* **2011**, *44* (17), 6653–6658.
- (16) Wu, W.-R.; Jeng, U.-S.; Su, C.-J.; Wei, K.-H.; Su, M.-S.; Chiu, M.-Y.; Chen, C.-Y.; Su, W.-B.; Su, C.-H.; Su, A.-C. Competition between fullerene aggregation and poly (3-hexylthiophene) crystallization upon annealing of bulk heterojunction solar cells. *ACS Nano* **2011**, *5* (8), 6233–6243.
- (17) Duong, D. T.; Ho, V.; Shang, Z.; Mollinger, S.; Mannsfeld, S. C. B.; Dacuña, J.; Toney, M. F.; Segalman, R.; Salleo, A. Mechanism of Crystallization and Implications for Charge Transport in Poly(3-ethylhexylthiophene) Thin Films. *Adv. Funct. Mater.* **2014**, *24* (28), 4515–4521.
- (18) Zheng, Y.; Wang, G.-J. N.; Kang, J.; Nikolka, M.; Wu, H.-C.; Tran, H.; Zhang, S.; Yan, H.; Chen, H.; Yuen, P. Y.; Mun, J.; Dauskardt, R. H.; McCulloch, I.; Tok, J. B.-H.; Gu, X.; Bao, Z. An Intrinsically Stretchable High-Performance Polymer Semiconductor with Low Crystallinity. *Adv. Funct. Mater.* **2019**, *29* (46), 1905340.
- (19) Aiyar, A. R.; Hong, J. I.; Izumi, J.; Choi, D.; Kleinhenz, N.; Reichmanis, E. Ultrasound-induced ordering in poly(3-hexylthiophene): role of molecular and process parameters on morphology and charge transport. *ACS Appl. Mater. Interfaces* **2013**, *5* (7), 2368–77.
- (20) Chang, M.; Choi, D.; Wang, G.; Kleinhenz, N.; Persson, N.; Park, B.; Reichmanis, E. Photoinduced Anisotropic Assembly of Conjugated Polymers in Insulating Polymer Blends. *ACS Appl. Mater. Interfaces* **2015**, *7* (25), 14095–103.
- (21) McBride, M.; Bacardi, G.; Morales, C.; Ristein, B.; Keane, D.; Reichmanis, E.; Grover, M. A. Control of Nucleation Density in Conjugated Polymers via Seed Nucleation. *ACS Appl. Mater. Interfaces* **2019**, *11* (41), 37955–37965.
- (22) Müller, C.; Zhigadlo, N. D.; Kumar, A.; Baklar, M. A.; Karpinski, J.; Smith, P.; Kreouzis, T.; Stingelin, N. Enhanced charge-carrier mobility in high-pressure-crystallized poly (3-hexylthiophene). *Macromolecules* **2011**, *44* (6), 1221–1225.
- (23) Cho, S.; Lee, K.; Yuen, J.; Wang, G.; Moses, D.; Heeger, A. J.; Surin, M.; Lazzaroni, R. Thermal annealing-induced enhancement of the field-effect mobility of regioregular poly (3-hexylthiophene) films. *J. Appl. Phys.* **2006**, *100* (11), 114503.
- (24) Fu, C. M.; Jeng, K. S.; Li, Y. H.; Hsu, Y. C.; Chi, M. H.; Jian, W. B.; Chen, J. T. Effects of Thermal Annealing and Solvent Annealing on the Morphologies and Properties of Poly (3-hexylthiophene) Nanowires. *Macromol. Chem. Phys.* **2015**, *216* (1), 59–68.
- (25) McBride, M.; Persson, N.; Keane, D.; Bacardi, G.; Reichmanis, E.; Grover, M. A. A Polymer Blend Approach for Creation of Effective Conjugated Polymer Charge Transport Pathways. *ACS Appl. Mater. Interfaces* **2018**, *10* (42), 36464–36474.
- (26) Diao, Y.; Tee, B. C.; Giri, G.; Xu, J.; Kim, D. H.; Becerril, H. A.; Stoltzenberg, R. M.; Lee, T. H.; Xue, G.; Mannsfeld, S. C.; Bao, Z. Solution coating of large-area organic semiconductor thin films with aligned single-crystalline domains. *Nat. Mater.* **2013**, *12* (7), 665–71.

- (27) Qu, G.; Zhao, X.; Newbloom, G. M.; Zhang, F.; Mohammadi, E.; Strzalka, J. W.; Pozzo, L. D.; Mei, J.; Diao, Y. Understanding Interfacial Alignment in Solution Coated Conjugated Polymer Thin Films. *ACS Appl. Mater. Interfaces* **2017**, *9* (33), 27863–27874.
- (28) Mohammadi, E.; Qu, G.; Kafle, P.; Jung, S.-H.; Lee, J.-K.; Diao, Y. Design rules for dynamic-template-directed crystallization of conjugated polymers. *Molecular Systems Design & Engineering* **2020**, *5* (1), 125–138.
- (29) Brinkmann, M.; Chandeson, F.; Pansu, R. B.; Julien-Rabant, C. Epitaxial growth of highly oriented fibers of semiconducting polymers with a shish-kebab-like superstructure. *Adv. Funct. Mater.* **2009**, *19* (17), 2759–2766.
- (30) Untilova, V.; Biskup, T.; Biniek, L.; Vijayakumar, V.; Brinkmann, M. Control of Chain Alignment and Crystallization Helps Enhance Charge Conductivities and Thermoelectric Power Factors in Sequentially Doped P3HT:F4TCNQ Films. *Macromolecules* **2020**, *53* (7), 2441–2453.
- (31) Boulanger, N.; Yu, V.; Hilke, M.; Toney, M. F.; Barbero, D. R. In situ probing of the crystallization kinetics of rr-P3HT on single layer graphene as a function of temperature. *Phys. Chem. Chem. Phys.* **2017**, *19* (12), 8496–8503.
- (32) Demir, F.; Van den Brande, N.; Van Mele, B.; Bertho, S.; Vanderzande, D.; Manca, J.; Van Assche, G. Isothermal crystallization of P3HT:PCBM blends studied by RHC. *J. Therm. Anal. Calorim.* **2011**, *105* (3), 845–849.
- (33) Yu, L.; Davidson, E.; Sharma, A.; Andersson, M. R.; Segalman, R.; Muller, C. Isothermal Crystallization Kinetics and Time-Temperature-Transformation of the Conjugated Polymer: Poly(3-(2'-ethyl)hexylthiophene). *Chem. Mater.* **2017**, *29* (13), 5654–5662.
- (34) Balko, J.; Rinscheid, A.; Wurm, A.; Schick, C.; Lohwasser, R. H.; Thelakkat, M.; Thurn-Albrecht, T. Crystallinity of poly(3-hexylthiophene) in thin films determined by fast scanning calorimetry. *J. Polym. Sci., Part B: Polym. Phys.* **2016**, *54* (18), 1791–1801.
- (35) Peng, Y.; He, Z.; Li, H.; Liang, C. Understanding the phase behavior from multiple-step isothermally crystallized poly(3-hexylthiophene)s. *Polymer* **2016**, *98*, 61–69.
- (36) Zhuravlev, E.; Schmelzer, J. W.; Wunderlich, B.; Schick, C. Kinetics of nucleation and crystallization in poly (ϵ -caprolactone)- (PCL). *Polymer* **2011**, *52* (9), 1983–1997.
- (37) Luo, S. C.; Kui, X.; Xing, E. R.; Wang, X. L.; Xue, G.; Schick, C.; Hu, W. B.; Zhuravlev, E.; Zhou, D. S. Interplay between Free Surface and Solid Interface Nucleation on Two-Step Crystallization of Poly(ethylene terephthalate) Thin Films Studied by Fast Scanning Calorimetry. *Macromolecules* **2018**, *51* (14), 5209–5218.
- (38) Davidson, E. C.; Segalman, R. A. Thermal Control of Confined Crystallization within P3EHT Block Copolymer Microdomains. *Macromolecules* **2017**, *50* (20), 8097–8105.
- (39) Zhuravlev, E.; Schick, C. Fast scanning power compensated differential scanning nano-calorimeter: 1. The device. *Thermochim. Acta* **2010**, *505* (1–2), 1–13.
- (40) Zhuravlev, E.; Schick, C. Fast scanning power compensated differential scanning nano-calorimeter: 2. Heat capacity analysis. *Thermochim. Acta* **2010**, *505* (1–2), 14–21.
- (41) Van den Brande, N.; Van Assche, G.; Van Mele, B. Isothermal structure development in submicron P3HT layers studied by fast scanning chip calorimetry. *Polymer* **2015**, *57*, 39–44.
- (42) Van den Brande, N.; Van Assche, G.; Van Mele, B. Fast scanning chip calorimetry study of P3HT/PC61BM submicron layers: structure formation and eutectic behaviour. *Polym. Int.* **2019**, *68* (2), 277–282.
- (43) Liu, Q.; Bottle, S. E.; Sonar, P. Developments of Diketopyrrolopyrrole-Dye-Based Organic Semiconductors for a Wide Range of Applications in Electronics. *Adv. Mater.* **2020**, *32* (4), 1903882.
- (44) Li, Y. N.; Sonar, P.; Murphy, L.; Hong, W. High mobility diketopyrrolopyrrole (DPP)-based organic semiconductor materials for organic thin film transistors and photovoltaics. *Energy Environ. Sci.* **2013**, *6* (6), 1684–1710.
- (45) Gumyusenge, A.; Tran, D. T.; Luo, X.; Pitch, G. M.; Zhao, Y.; Jenkins, K. A.; Dunn, T. J.; Ayzner, A. L.; Savoie, B. M.; Mei, J. Semiconducting polymer blends that exhibit stable charge transport at high temperatures. *Science* **2018**, *362* (6419), 1131–1134.
- (46) Venkateshvaran, D.; Nikolla, M.; Sadhanala, A.; Lemaur, V.; Zelazny, M.; Kepa, M.; Hurhangee, M.; Kronemeijer, A. J.; Pecunia, V.; Nasrallah, I.; Romanov, I.; Broch, K.; McCulloch, I.; Emin, D.; Olivier, Y.; Cornil, J.; Beljonne, D.; Sirringhaus, H. Approaching disorder-free transport in high-mobility conjugated polymers. *Nature* **2014**, *515* (7527), 384–388.
- (47) Reiter, G. Some unique features of polymer crystallisation. *Chem. Soc. Rev.* **2014**, *43* (7), 2055–2065.
- (48) Luo, S. C.; Wang, T. Y.; Ocheje, M. U.; Zhang, S.; Xu, J.; Qian, Z. Y.; Gu, X. D.; Xue, G.; Rondeau-Gagne, S.; Jiang, J.; Hu, W. B.; Zhuravlev, E.; Zhou, D. S. Multiamorphous Phases in Diketopyrrolopyrrole-Based Conjugated Polymers: From Bulk to Ultrathin Films. *Macromolecules* **2020**, *53* (11), 4480–4489.
- (49) Van den Brande, N.; Van Assche, G.; Van Mele, B. Thermal behaviour below and inside the glass transition region of a submicron P3HT layer studied by fast scanning chip calorimetry. *Polymer* **2016**, *83*, 59–66.
- (50) Minakov, A. A.; Schick, C. Ultrafast thermal processing and nanocalorimetry at heating and cooling rates up to 1MK/s. *Rev. Sci. Instrum.* **2007**, *78* (7), 073902.
- (51) Yin, J.; Raegen, A.; Idziak, S. H. J.; Forrest, J. A. Crystallization and melting of highly monodisperse poly(ethylene-oxide). *Soft Matter* **2020**, *16* (34), 7958–7969.
- (52) Wunderlich, B. Reversible crystallization and the rigid-amorphous phase in semicrystalline macromolecules. *Prog. Polym. Sci.* **2003**, *28* (3), 383–450.
- (53) Beckingham, B. S.; Ho, V.; Segalman, R. A. Formation of a Rigid Amorphous Fraction in Poly(3-(2'-ethyl)hexylthiophene). *ACS Macro Lett.* **2014**, *3* (7), 684–688.
- (54) Avrami, M. Kinetics of Phase Change. II Transformation-Time Relations for Random Distribution of Nuclei. *J. Chem. Phys.* **1940**, *8* (2), 212–224.
- (55) Choi, D.; Chang, M.; Reichmanis, E. Controlled Assembly of Poly(3-hexylthiophene): Managing the Disorder to Order Transition on the Nano- through Meso-Scales. *Adv. Funct. Mater.* **2015**, *25* (6), 920–927.
- (56) Jiemsakul, T.; Jiramitmongkon, K.; Asawapirom, U.; Chotsawan, C. Investigation of P3HT electrochromic polymer films prepared by ultrasonication of polymer solutions. *J. Mater. Sci.* **2017**, *52* (14), 8485–8492.
- (57) Meldrum, F. C.; O'Shaughnessy, C. Crystallization in Confinement. *Adv. Mater.* **2020**, *32* (31), 2001068.
- (58) Baker, J. L.; Jimison, L. H.; Mannsfeld, S.; Volkman, S.; Yin, S.; Subramanian, V.; Salleo, A.; Alivisatos, A. P.; Toney, M. F. Quantification of Thin Film Crystallographic Orientation Using X-ray Diffraction with an Area Detector. *Langmuir* **2010**, *26* (11), 9146–9151.